J Appl Electrochem (2008) 38:51–62
DOI 10.1007/s10800-007-9398-x

ORIGINAL PAPER

Direct methanol fuel cells with reticulated vitreous carbon, uncompressed graphite felt and Ti mesh anodes

Tommy T. Cheng · Előd L. Gyenge

Received: 6 February 2007 / Revised: 25 June 2007 / Accepted: 14 August 2007 / Published online: 8 September 2007

Abstract Reticulated vitreous carbon (RVC, 39 pores per cm), uncompressed graphite felt (UGF) and Ti mesh were investigated as 3-D anode catalyst supports for direct liquid methanol fuel cells with the aim of improving the catalyst mass specific activity. Mesoporous Pt–Ru layers composed of nano-particle agglomerates were electrodeposited on the 3-D substrates using a micellar deposition media composed of Triton X-100, isopropanol, and an aqueous phase containing H_2PtCl_6 and $(NH_4)_2RuCl_6$. The effect of deposition current density, support type, and counter electrode design on the catalyst layer morphology, mass loading and elemental composition is discussed. In direct methanol fuel cell experiments using 1 M CH_3OH—0.5 M H_2SO_4 the 3-D anodes with PtRu load between 2.8 g m^{-2} (on Ti mesh) and 12.0 g m^{-2} (on RVC) and Pt:Ru atomic ratio of about 4:1 provided peak power outputs based on catalyst mass of 50.4 W g^{-1} and 40.5 W g^{-1}, respectively, at 333 K. The mass specific activity of the catalyst supported on the 3-D matrix is determined by the synergy between catalyst deposition procedure and support physico-chemical properties.

Keywords Electrocatalysts · Methanol electro-oxidation · Electrodeposition · Three-dimensional electrodes

T. T. Cheng · E. L. Gyenge (✉)
Department of Chemical and Biological Engineering,
The University of British Columbia, 2360 East Mall, Vancouver,
BC, Canada V6T 1Z3
e-mail: egyenge@chml.ubc.ca

1 Introduction

The direct methanol fuel cell (DMFC) has attracted much research attention over the past two decades due to its high theoretical energy density (4.8 kWh l^{-1}) and potential suitability as power source for both automotive transportation and portable electronic devices as a consequence of simpler, liquid-based, fuelling infrastructure [1]. However, the sluggish CH_3OH electro-oxidation kinetics coupled with catalytic activity loss over time due mainly to the accumulation of the CO intermediate on the Pt catalyst surface (e.g. the reaction rate decreases by a factor of four to five during the first 100 ms of reaction [2]) remains a major challenge even after four decades of methanol electro-oxidation research, hampering the commercialization of the DMFC. PtRu catalysts acting most likely by a combination of bifunctional mechanism and electronic coordination effect, with optimal Pt:Ru atomic ratios between 1:1 and 4:1 (depending on temperature, electrode potential and CH_3OH concentration), show lower susceptibility for CO poisoning and higher CH_3OH oxidation rates at low anode potentials (e.g. below 0.6 V vs. SHE). Moreover, PtRu catalysts enhance the complete 6 e^- electro-oxidation rate compared to pure Pt.

The area of CH_3OH electro-oxidation kinetics and catalysis has been extensively discussed [3–6]. The slow anode kinetics causing a low CH_3OH conversion per pass in the thin catalyst layer (thickness about 20 μm) of the gas diffusion electrode contributes indirectly to the enhanced CH_3OH diffusion across the solid polymer electrolyte, which in turn compromises the cathode performance by establishment of a mixed potential on the cathode surface [7, 8].

In addition to fundamental electrocatalytic aspects and development of improved electrocatalyst formulations (e.g.

ternary and quaternary compositions such as Pt–Ru–Rh–Ni [9], Pt–Ru–Os–Ir [10]) the synergy between the catalyst layer and the overall anode structure (e.g. presence and/or type of support, catalyst-support interaction, ionic conductor load, hydrophobic-hydrophilic pore balance) has a significant impact on the fuel cell performance-catalyst load (i.e. cost) relationship. The utilization of the catalyst load in a typical membrane-gas diffusion electrode assembly, defined as the ratio between the effective electrochemically available surface area and the total catalyst surface area, is between 10 and 50% [11] and it could further diminish during extended fuel cell operation. Furthermore, the counter-current two-phase (L: CH_3OH and H_2O; G: CO_2) flow in the porous electrode affects the diffusion overpotential and the effective ionic conductivity [12].

Whilst numerous studies have been devoted to understanding and improving the electrocatalysis of CH_3OH oxidation, the engineering of both the catalyst layer and the overall anode structure has received much less attention. The vast majority of DMFC experiments have been carried out with gas diffusion type anodes comprising of carbon cloth or paper diffusion-backing layer and carbon-black supported catalyst layer containing Nafion ionic conductor. Mastragostino et al. showed the importance of optimizing the anode catalyst layer composition for DMFCs with respect to Nafion load and type of carbon support together with their combined effect on the electrochemically available surface area [13]. Utilizing carbon nanocoil supported PtRu (1:1) catalyst promising DMFC results were obtained by Hyeon et al. with a load of 20 g m^{-2} (e.g. peak power density of 2300 W m^{-2} was achieved at 333 K) [14].

Wilkinson et al. recognized the importance of the anode design in reducing the methanol crossover, and they patented the multi-layer anode concept [15]. Three sheets of carbon fiber paper (thickness 100 μm) with PtRu supported on carbon black applied onto them (total load of 18 g m^{-2}) were stacked to give a multi-layer DMFC anode. Employing a constant volume of 250 mL 2 M CH_3OH-0.5 M H_2SO_4 they found that the methanol utilization increased from 60 to 80% with the multi-layer anode compared to a single-layer electrode. Recently, Gyenge and collaborators proposed three-dimensional monolithic carbon-based electrodes of about 200 to 2,000 μm thickness, as direct alcohol fuel cell anodes [16–18]. The three-dimensional matrix supporting well-dispersed electrocatalysts with various morphologies such as discreet nano-particles or thin mesoporous coatings (pore diameter between 2 and 50 nm according to IUPAC nomenclature [19]) could assure an extended reaction zone for CH_3OH oxidation compared to the gas diffusion design providing an ionic (i.e. H_3O^+) conductor network is established to link the catalytically active sites and the proton exchange membrane. Both the multi-layer and the three-dimensional anode concepts are similar since they provide an extended reaction zone (volume) for the electrochemical reaction. However, the monolithic three-dimensional electrode eliminates the possible contact resistance between the individual layers.

Structural differences and surface physico-chemical properties of the three-dimensional electrode matrices such as various graphite felts and reticulated vitreous carbons, could improve the two-phase (L/G) flow dynamics. Three-dimensional electrodes can accommodate a wide range of L/G flow regimes [20] as opposed to the gas diffusion electrode, which operates best in the gas continuous regime and therefore, is susceptible to flooding. These issues would gain significance with scale-up of DMFC (e.g. to geometric electrode areas of 25–100 cm^2) and large stack development.

The three-dimensional electrode concept poses two major challenges. The first one relates to synthesizing and uniformly depositing nano-sized electrocatalyst throughout the thickness of the three-dimensional matrix. The second challenge is the formation of the proton conductor network across the three-dimensional electrode connecting the electrocatalytic sites and the PEM membrane, as discussed also by Wilkinson et al. [15].

In order to address the first challenge, the goal of the present investigation was to study the electrodeposition of Pt–Ru nanostructures on different three-dimensional electrodes, namely, reticulated vitreous carbon (RVC), uncompressed graphite felt (UGF) and Ti mesh, using colloidal deposition media to control the crystallite size [17]. Furthermore, the larger aim of this study was to determine the applicability of the various three-dimensional substrates as DMFC anodes by a combination of fundamental electrochemical and surface analytical techniques in conjunction with fuel cell experiments. The issue of protonic conductivity in the fuel cell anode was addressed by employing a liquid electrolyte, 0.5 M H_2SO_4—1 M CH_3OH solution. While the liquid electrolyte serves the purpose of demonstrating the concept of three-dimensional fuel cell electrodes, further studies are required to investigate the possibility of forming a solid electrolyte network with sufficient protonic conductivity across the thickness of the extended reaction zone anode.

2 Experimental section

2.1 Three-dimensional catalyst supports and their pretreatment

The three-dimensional electrodes employed in the present work were: reticulated vitreous carbon (RVC, Electrolytica

Inc., 39 pores per centimeter, thickness 2×10^{-3} m), uncompressed graphite felt (UGF, Test Solutions, thickness 3×10^{-3} m) and Ti mesh (VWR Canlab, 2×10^{-4} m). Figure 1 shows the SEM images of the electrode surfaces.

We have shown previously the importance of RVC pretreatment for nanostructure electrodeposition [17]. Table 1 summarizes the pretreatment methods applied for the different supports. The electrochemical pretreatment method involved potential cycling of the RVC between 1.44 and 2.09 V versus SHE in concentrated H_2SO_4 solution (see Table 1) at a scan rate of 1 mV s^{-1} repeated 50 times [17]. The electrochemical pretreatment could not be carried out on UGF due to severe weakening of the physical integrity of the material. Therefore, the only pretreatment applied to the felt electrode was sonication in methanol for 30 min. The pretreatment method for Ti mesh involved etching in boiling HCl for 30 s to remove the well-adhered surface oxide layer [21]. Upon pretreatment, all samples (5×10^{-4} m^2 geometric area) were washed thoroughly with distilled water followed by drying in air.

Table 1 Substrate pretreatment methods

Substrate	Electrochemical cycling in concentrated sulfuric acid	Sonication in methanol	Etching in boiling hydrochloric acid
RVC	+	–	–
UGF	–	+	–
Ti Mesh	–	–	+

2.2 Electrodeposition procedure

Two colloidal electrodeposition media were investigated and compared, a novel micellar solution and a microemulsion system discussed previously [17]. The micellar deposition solution was composed of Triton X-100 nonionic surfactant [$C_8H_{17}C_6H_4O(C_2H_4O)_{9.5}H$], iso-propanol, and an aqueous phase with various concentrations of H_2PtCl_6 and $(NH_4)_2RuCl_6$. A typical deposition bath had the following composition: 5 vol.% Triton X-100, 20 vol.% iso-propanol, and 75 vol.% aqueous phase with H_2PtCl_6 and $(NH_4)_2RuCl_6$. The concentration of the Pt and Ru compounds was of 2.5×10^{-4} M each in the total colloidal solution. In Sect. 3.1 further details are given regarding the role of isopropanol and a comparison is made with the microemulsion and pure aqueous deposition media. The chemicals used were reagent grade obtained from Sigma-Aldrich and were used as delivered without further purification processes. The micellar solutions were prepared by mixing the aqueous and surfactant phases in a water-jacketed glass vessel connected to a circulating water bath at 341 K for 30 min.

The electrode assembly composed of the working electrode (geometric area of 5×10^{-4} m^2) placed at a distance of 10^{-2} m between two Pt/Ti counter electrodes (5×10^{-4} m^2 geometric area each) was inserted into the glass vessel and connected to a dc power supply (Xantrex XHR150-7 DC Power Supply, 0–150 V, 0–7 A) to carry out the electrodeposition.

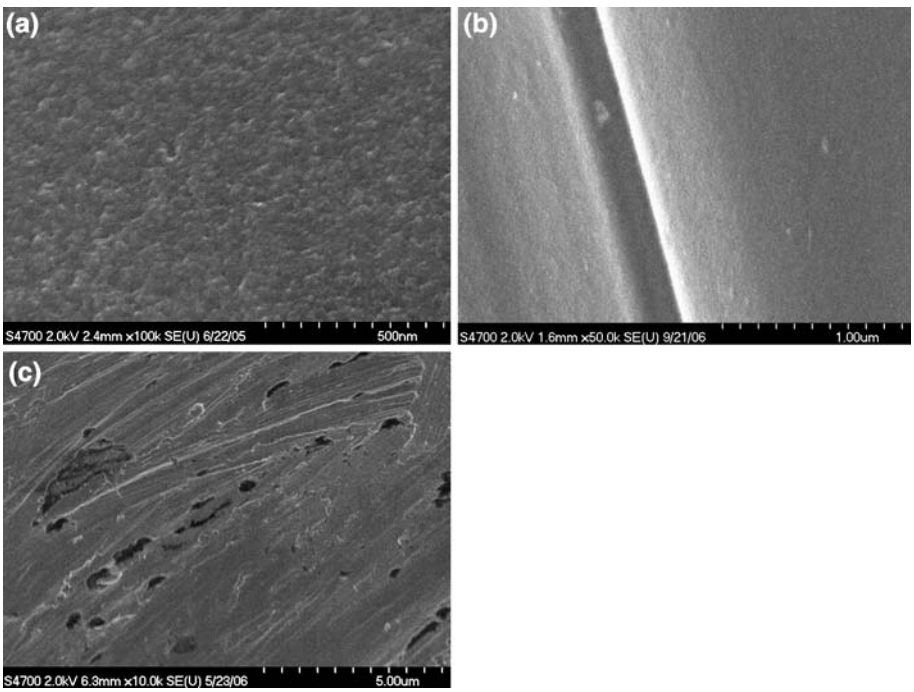

Fig. 1 SEM images of (**a**) RVC, (**b**) UGF, and (**c**) Ti mesh surfaces

After the deposition experiment was completed, the working electrode was sonicated in tetrahydrofuran (THF) (Reagent Grade, Sigma Aldrich) for 5 min to wash out the organic compounds retained in the porous matrix. The deposited substrate was then washed thoroughly with distilled water and dried, followed by heat treatment in a N_2 stream for 1 h at 573 K to remove traces of adsorbed organic compounds [17].

2.3 Electrochemical measurements

Voltammetry (CV) was carried out at 298 K, with a three-electrode setup, in a water-jacketed electrochemical cell connected to a circulating water bath. The test solution was 1.0 M CH_3OH and 0.5 M H_2SO_4 with a volume of 50 mL. The Hg/Hg_2SO_4, $K_2SO_{4,\ std.}$ (MSE) electrode and a platinum wire were used as reference and counter electrodes, respectively. A computer-controlled VoltaLab PGZ402 potentiostat with the VoltaMaster 4 software by Radiometer Analytical was used in the experiments. All potentials in the present work are reported against the standard hydrogen electrode (SHE) reference.

The catalyst surface was chemically and electrochemically pre-treated to remove surface impurities. The chemical pretreatment involved the immersion of the working electrodes in a 1:1 v/v. concentrated H_2SO_4 and 30 vol.% H_2O_2 (Fisher Scientific) solution five times for a few seconds each, and rinsed thoroughly with distilled water. Following the chemical pretreatment, the working electrodes were cleaned three times in 0.5 M H_2SO_4 by applying potential steps for 10 s each at 1.28, 1.20 and 0.05 V, respectively.

The effective electrochemically active PtRu surface area was estimated by the Cu underpotential deposition and anodic stripping technique [17, 22]. In our previous investigations we found that Cu does not underpotentially deposit on vitreous carbon [17]. Therefore, assuming complete Cu monolayer coverage on the Pt and Ru sites, the effective surface area can be calculated from the anodic stripping charge (i.e. 4.2 C m^{-2}).

Reference voltammograms in the range –0.04 to 0.91 V were first obtained in 0.5 M H_2SO_4 at a scan rate of 50 mV s^{-1}. The Cu UPD experiments were carried out in 0.5 M H_2SO_4 and 2 mM $CuSO_4$ at 298 K. The underpotential deposited Cu monolayer was formed on the catalyst surface by polarizing the working electrodes at 0.26 V for 300 s. Afterwards, a linear voltammetric scan in the anodic direction was applied between 0.26 and 0.91 V with a scan rate of 50 mV s^{-1} to remove the adsorbed copper monolayer. The charge differences in the same potential range between the reference scan and Cu stripping were used to calculate the active surface area.

2.4 Surface and analytical characterization of the catalysts

Hitachi S4700 high resolution scanning electron microscope (SEM) was used to capture visual images of the prepared catalysts. Fragments of the deposited substrates were flush mounted onto SEM stubs with carbon adhesive. An accelerating voltage and emission current of 2,000 V and 1.25×10^7 A, respectively, were employed at a working distance of 0.0025–0.0035 m to obtain the images. Inductively coupled plasma atomic emission spectroscopy (ICP-AES) using a Perkin Elmer Optima, model 3300DV instrument, was used to determine the mass loading of the electrodeposits.

2.5 Membrane electrode assembly and fuel cell experiments

The membrane electrode assembly (MEA) was prepared with a half MEA (cathode, Fideris Inc., Nafion® 117 membrane) with 40 g m^{-2} of pre-painted Pt black and the 3-D anode (5×10^{-4} m^2). The DMFC was assembled with two gold-plated end plates, an Elat® carbon cloth (E-Tek Inc.) as the cathode backing layer, the custom MEA with the 3-D anode, a silicone-coated gasket, and a carbon cloth as the anode backing layer. The DMFC was held together by insulated bolts.

The fuel cell tests were performed using a Fideris Inc. MTK fuel cell test station, equipped with corrosion-resistant fittings and operated using the FC Power® software. The fuel cell tests were carried out at 333 K with an oxygen flow rate of 500 mL min^{-1} at 2.5 bar absolute pressure. Dry medical grade oxygen was used as supplied by Praxair Inc. The anode was fed with a solution of 0.5 M H_2SO_4 and 1 M CH_3OH at 2 mL min^{-1} full recycle. With the flow system and temperature control turned on at open circuit, membrane conditioning was performed for 2 h. This step assured a stable and reproducible operation of the cell. Current was then progressively drawn and the cell voltage was recorded after 2 min of continuous operation at constant current

3 Results and discussion

3.1 Electrodeposition from micellar solution versus microemulsion: RVC support

In our previous work a microemulsion media was investigated for the galvanostatic electrodeposition of PtRu on RVC. The microemulsion was composed of 72 vol.% cyclohexane (with 10^{-3} M tetrabutylammonium

perchlorate), 25 vol.% mixture of Triton X-100 and isopropanol in 1:4 volume ratio, and 3 vol.% aqueous phase with 0.01 M H_2PtCl_6 and $(NH_4)_2RuCl_6$ [17]. The galvanostatic deposition mode was chosen instead of the controlled potential variant, for superior industrial applicability. Moreover, the constant deposition current density could also assure better reproducibility of the catalyst mass load throughout the three-dimensional electrode structure. Due to the very low ionic conductivity of the microemulsion (i.e. 2×10^{-5} S m^{-1}) the deposition current density was limited to 10 A m^{-2}, generating a PtRu load on RVC of 2.3 g m^{-2} in 234 min at 341 K. The Pt:Ru atomic ratio was 1.3:1. Comparative PtRu electrodeposition in an aqueous solution carried out under identical conditions of surface pretreatment, deposition current density, temperature and time, yielded a Pt rich catalyst (Pt:Ru atomic ratio of 15:1) with much lower catalyst load (i.e.1 g m^{-2}) and mass specific surface area (24 vs. 40 m^2 g^{-1}) [17]. Thus, the presence of a colloidal system and a surfactant in particular are essential to control the catalyst load and composition (Pt:Ru ratio) on the three-dimensional substrate as it was also conclusively demonstrated in previous work from this group [16].

The goal here was to simplify the colloidal electrodeposition bath composition while further improving the electrocatalytic activity by affecting the catalyst morpholgy and Pt:Ru ratio. Therefore, a new deposition bath was developed without the presence of cyclohexane, the majority component in the previously employed microemulsion system. The non-ionic surfactant Triton X-100 and isopropanol were retained in order to create a micellar deposition media containing aqueous H_2PtCl_6 and $(NH_4)_2RuCl_6$. Teh et al. reported that isopropanol eliminates the possible formation of liquid crystal gel in the Triton X-100/aqueous system, forming a micellar solution instead [23, 24]. The hydrodynamic radius of the micelles decreased by the addition of isopropanol and further decrease was observed with increased temperature at isopropanol concentration of 14 to 26 wt.%. For example, the hydrodynamic radius at 293 K decreased from 4.13 nm (0 wt.% isopropanol) to 1.95 nm (26 wt.%). At 298 K and 26 wt.% isopropanol, the hydrodynamic radius was 1.74 nm [23, 24].

In our current study, the micellar system was composed of 75 vol.% aqueous phase and 25 vol.% Triton X-100/isopropanol in a 1:4 volume ratio. The weight percentages were: 6 wt.% Triton X-100 and 17 wt.% isopropanol.

Comparative galvanostatic electrodeposition experiments were performed in the two media, i.e. microemulsion and micellar, with 2.5×10^{-4} M H_2PtCl_6 and $(NH_4)_2RuCl_6$ each. The deposition superficial current density was 10 A m^{-2}, applied continuously for 240 min at a constant temperature of 341 K. Table 2 shows the PtRu

Table 2 Electrodeposition of PtRu on RVC from colloidal media: comparison between micellar and microemulsion methods. Electrodeposition conditions: 10 A m^{-2}, 240 min, 341 K, flat plate counter electrodes

Deposition media	Mass loading (g m^{-2})	Bulk Pt:Ru atomic ratio	Specific surface area (m^2 g^{-1})
Microemulsion	2.3	1.3:1	40
Micellar	1.5	7.3:1	46

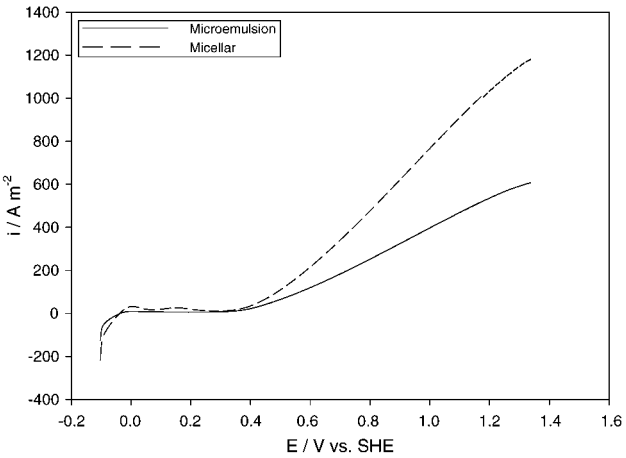

Fig. 2 Voltammograms of methanol electro-oxidation using PtRu electrodeposited on RVC: Effect of colloidal electrodeposition media.1 M CH_3OH and 0.5 M H_2SO_4. Temperature: 298 K. Scan rate: 5 mV s^{-1}

characteristics obtained, while Fig. 2 compares the electrocatalytic activity toward methanol oxidation by voltammetry.

The methanol electro-oxidation superficial current density on PtRu/RVC at 298 K was higher for the catalyst prepared by electrodeposition from micellar media compared to microemulsion (Fig. 2). This result is interesting considering the lower catalyst load obtained using the micellar media (1.5 g m^{-2}) and the approximately identical specific surface area of the two catalysts (Table 2). High resolution SEM showed (Fig. 3) that the micellar solution produced a more porous, interconnected open cell deposit morphology compared to the denser particulate-like structure due to microemulsion. However, these apparent morphological differences were not reflected in the measured specific surface area by the Cu UPD technique.

Changing the phase structure of the electrodeposition media affected not only the deposit load and morphology but also the Pt:Ru atomic ratio (Table 2).The micellar system produced a catalyst with high Pt:Ru atomic ratio 7.3:1, whilst the microemulsion favored more the Ru deposition generating a Pt:Ru ratio of 1.3:1. This could explain the differences in electrocatalytic activity observed by voltammetry at 298 K (Fig. 2). The optimal Pt:Ru ratio

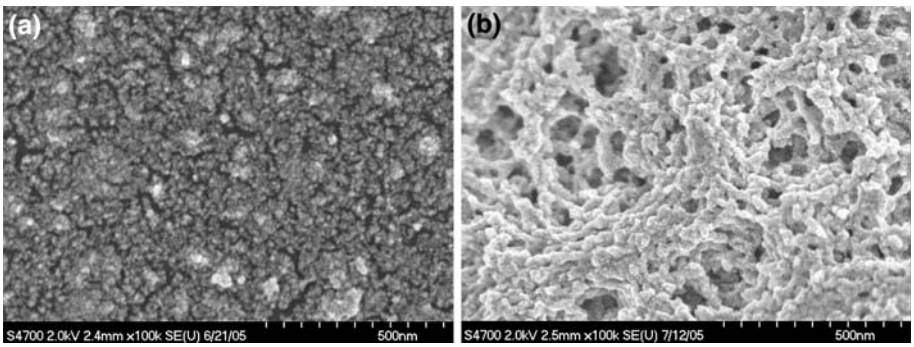

Fig. 3 SEM images of electrodeposited PtRu on RVC prepared with microemulsion and micellar solution. (**a**) Microemulsion; (**b**) Micellar solution

is a long-standing issue in the methanol electro-oxidation literature. Gasteiger et al. found using ultra-high vacuum experiments on sputter-cleaned alloys, that surfaces with 7–10 at.% Ru are the most active at room temperature, with a shift to 50 at.% Ru at high temperatures (e.g. 333 K) due to a change in the rate determining step from adsorption/dehydrogenation of CH_3OH to oxidation of CO_{ads} [25–27]. Therefore, the capability to easily control the Pt:Ru ratio by adjusting certain variables of the catalyst preparation procedure (such as solution composition, deposition current density, temperature and electrode geometry) is of paramount significance. Further experiments were carried out using the micellar deposition media aimed at controlling both the catalyst load and the Pt:Ru atomic ratio.

3.2 PtRu electrodeposition on RVC using the micellar media: effect of perforated counter electrodes and deposition current density

During electrodeposition significant O_2 gas evolution occurs on the counter electrodes. The inefficient release of gas bubbles from the cell decreases the effective conductivity and therefore, alters the potential distribution which impacts the deposit characteristics such as load, morphology and penetration throughout the three-dimensional matrix. In order to improve the gas disengagement on the counter electrodes, perforated Pt/Ti plates were employed with 10 holes per cm^2 and hole dimension of about 3 mm^2.

For a deposition superficial current density of 10 A m^{-2} applied for 240 min at 341 K, the perforated counter electrode design yielded on the RVC substrate a three fold increase of Pt:Ru mass loading from 1.5 to 4.6 g m^{-2} (Table 3). The Pt:Ru ratio in the deposit was found to be 7.2:1, virtually identical to the catalyst sample produced without the use of perforated counter electrodes. Moreover, the catalyst morphology remained the same as shown by SEM imaging (compare Figs. 4a and 3b). However, the specific surface area decreased to 29 m^2 g^{-1} indicating the build up of a thicker film.

The catalyst produced with perforated counter electrodes showed enhanced activity toward CH_3OH electro-oxidation compared to the one obtained using unperforated, flat, counter electrodes (Fig. 5 curves A and B). This is likely due to the higher catalyst surface area enhancement factor a_s (defined as the total catalyst surface area per geometric area of the substrate, Eq. 1), i.e. 133 m^2 m^{-2} versus 69 m^2 m^{-2} for the catalysts produced with perforated versus flat counter electrodes, respectively.

$$a_s = a_m \cdot m_c, \tag{1}$$

where a_s is the area enhancement factor defines as the total catalyst area per geometric area of the substrate (electrode) (m^2_{total} m^{-2}_{geom}), a_m is the mass specific catalyst surface area (m^2_{total} g^{-1}) and m_c is the catalyst load (g m^{-2}_{geom}).

The application of higher deposition current density (20, 40, and 60 A m^{-2} vs. 10 A m^{-2}), which was permitted by the high ionic conductivity of the micellar solution and more effective gas release due to the perforated counter

Table 3 Effect of perforated counter electrodes on the electrodeposition of PtRu from micellar solution on various three-dimensional substrates. Temperature 341 K

Substrate	Deposition current density (A m^{-2})	Time (min)	Mass loading (g m^{-2})	Bulk Pt:Ru atomic ratio	Specific surface area (m^2 g^{-1})
RVC	10	240	4.6	7.2:1	29
RVC	20	120	12.0	3.6:1	12
RVC	40	60	8.7	4.4:1	16
RVC	60	40	4.9	3.5:1	25
UGF	20	120	9.8	4.0:1	36
Ti mesh	20	120	2.8	4.5:1	32

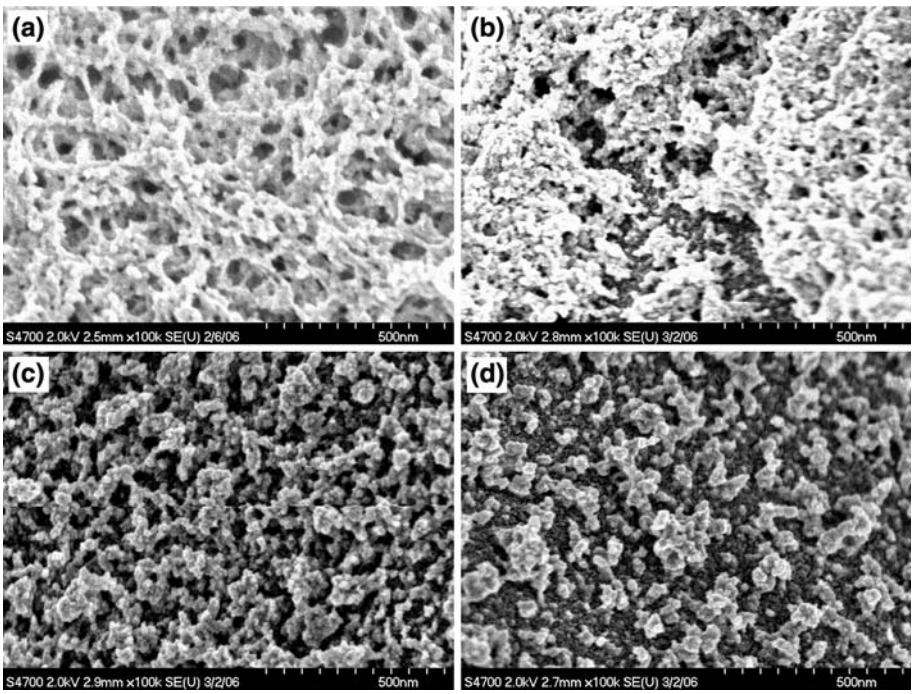

Fig. 4 SEM images of electrodeposited PtRu on RVC prepared from micellar solution with perforated counter electrodes at 341 K. Effect of deposition current density (**a**) 10 A m^{-2}; (**b**) 20 A m^{-2}; (**c**) 40 A m^{-2}; (d) 60 A m^{-2}

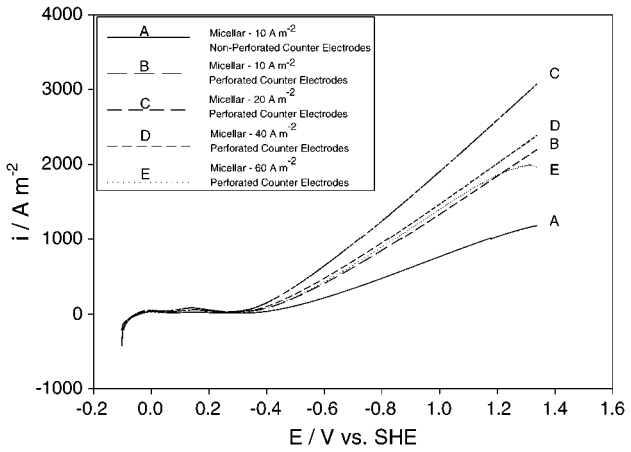

Fig. 5 Voltammograms of methanol electro-oxidation using PtRu electrodeposited on RVC. Effect of electrodeposition conditions: counter electrode type and superficial current density. 1 M CH_3OH and 0.5 M H_2SO_4. Temperature: 298 K. Scan rate: 5 mV s^{-1}

electrode, was found to have significant effects on the catalyst morphology, total load and Pt:Ru ratio (Table 3). Interestingly, whilst the total charge applied during deposition remained the same, the deposit mass load on RVC changed with superficial current density, up to 12 g m^{-2} at 20 A m^{-2} and the Pt:Ru atomic ratio decreased to 3.5:1 at 60 A m^{-2} (Table 3). Therefore, the higher current density favored the electrodeposition of Ru from the micellar solution. However, the Pt:Ru atomic ratio leveled off to ~4:1 and a further increase in current density above 20 A m^{-2} did not have a significant impact on the Ru deposition. The surface area enhancement factor (Eq. 1) on RVC was the highest for the catalyst prepared at 20 A m^{-2} compared to the 10 A m^{-2} case, i.e. 144 m^2 m^{-2} versus 133 m^2 m^{-2}, respectively. The deposit morphology at 20 A m^{-2} was characterized by a mesoporous structure (pore diameter equal or less than 50 nm), formed by interconnected nanoparticles of approximately 10–20 nm diameter (Fig. 4b). At 40 A m^{-2}, the mesoporous structure began to disappear and completely vanished at 60 A m^{-2}. The resulting morphology was a rough catalyst coating made up of particles of 20–50 nm diameter (Fig. 4c and d).

Figure 5 shows the catalyst prepared at 20 A m^{-2} using perforated counter-electrodes gave the highest anodic current densities at 298 K for 1 M CH_3OH oxidation in 0.5 M H_2SO_4. This result is in accordance with the surface area enhancement factor, however, the contribution of the different Pt:Ru atomic ratio cannot be disregarded (Table 3).

3.3 Effect of catalyst support

Micellar electrodeposition of PtRu was carried out on RVC, UGF and Ti Mesh supports. The experiments were carried out at 341 K with a deposition superficial current density and time of 20 A m^{-2} and 120 min, respectively. The mass loading, Pt:Ru ratio, and specific surface area (determined by Cu UPD and stripping) of the catalysts prepared on the different substrates are presented in Table 3.

The highest mass loading was obtained with the RVC support 12 g m^{-2}, which was attributed to the large number

of deposition sites created by the electrochemical cycling pretreatment method as shown previously [17]. On graphite felt the load was lower, 9.8 g m^{-2}, since surface pretreatment could not be carried out due to a loss of mechanical integrity. The load on Ti mesh was only 2.8 g m^{-2} due probably to incomplete removal of the non-conductive surface oxide layer and/or incomplete wetting of the surface by the micellar media.

The morphology of the deposits on all three supports could be characterized as mesoporous coating composed of nanoparticle agglomerates (Fig. 6). The highest catalyst surface area enhancement factor was obtained in the case of UGF (i.e. 352.8 m^2 m^{-2} compared to 144 m^2 m^{-2} for RVC and 89.6 m^2 m^{-2} for Ti mesh). The Pt:Ru ratio varied only slightly with deposition substrate type, in the range of 3.5:1 to 4.5:1 (Table 3).

Interestingly, voltammetric experiments carried out at 298 K revealed the highest CH_3OH electro-oxidation superficial current density for to the RVC supported catalyst, followed by UGF, and lastly Ti mesh (Fig. 7). Thus, the order of electrocatalytic activity between RVC and UGF did not follow the catalyst surface area enhancement factor a_s. This indicates that there must be more subtle differences between the PtRu catalysts supported on RVC and UGF, respectively.

In order to demonstrate differences between the PtRu/RVC and PtRu/UGF systems, we express the superficial current density for methanol oxidation i (A m^{-2}_{geom}) in the three-dimensional electrode in terms of catalyst physico-chemical properties, catalyst utilization efficiency and local current density:

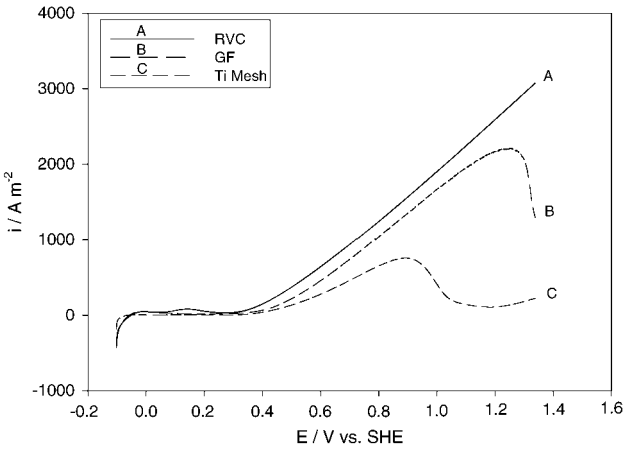

Fig. 7 Effect of three-dimensional support on the electrocatalytic activity of PtRu for methanol electro-oxidation. Voltammograms in 1 M CH_3OH and 0.5 M H_2SO_4. Temperature: 298 K. Scan rate: 5 mV s^{-1}. Samples prepared at a temperature of 341 K and a deposition current density of 20 A m^{-2} for 120 min with perforated counter electrodes in micellar solution

$$i = \gamma_c \cdot a_v \int_0^{\tau} i_j dx = \gamma_c \cdot a_m \frac{m_c}{\tau} \int_0^{\tau} i_j dx \qquad (2)$$

where a_v is the volume specific catalyst surface area (i.e. the total catalyst area as determined by off situ physico-chemical/electrochemical methods per geometric volume of the three-dimensional electrode (m^2_{total} m^{-3}_{geom})), a_m is the catalyst surface area per unit catalyst weight (referred to as the mass specific surface area (m^2_{total} g^{-1})), i_j is the local current density (A m^{-2}_{eff}), m_c is the catalyst load (g m^{-2}_{geom}),

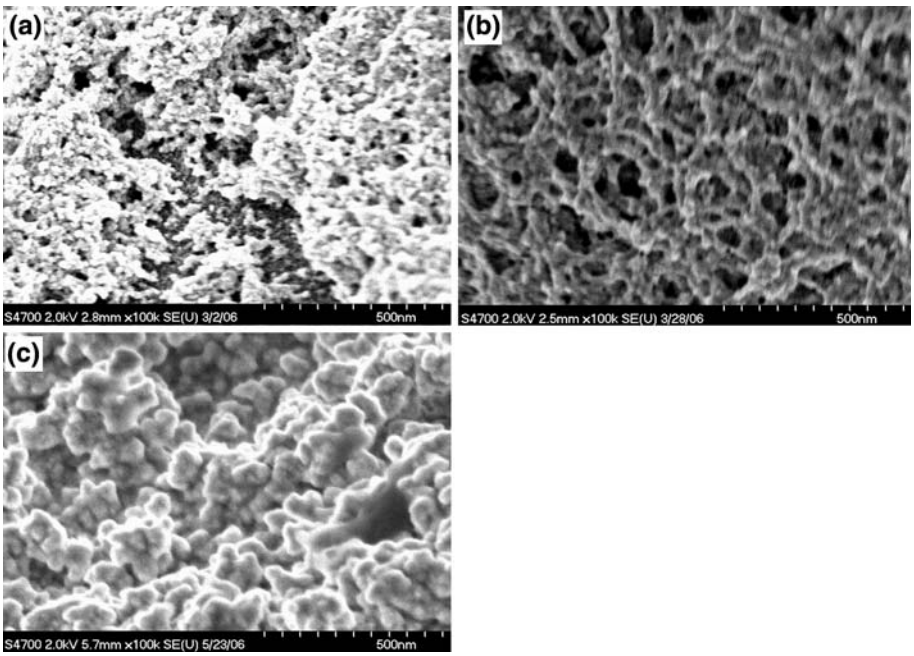

Fig. 6 SEM images of PtRu electrodeposits prepared from micellar solution with different substrates at 20 A m^{-2}, 341 K and perforated counter electrodes. Support type: (**a**) RVC; (**b**) UGF; (**c**) Ti Mesh

γ_c is the catalyst utilization efficiency reflecting the effective area participating in the electrochemical reaction ($m^2_{eff}\ m^{-2}_{total}$), and τ is the electroactive reaction zone (or catalyst layer) thickness (m_{geom}). Note that τ may or may not be equal to the physical thickness of the three-dimensional electrode, depending on the catalyst deposition penetration across the thickness and the availability of the ionic conductor network linking the catalytic sites.

The local current density i_j is related to the local anode overpotential η_j according to various electrode polarization conditions, such as intrinsic electrode kinetic control, or mixed control involving intrinsic electrode kinetics together with reactant mass transfer and/or ionic conductivity effects leading to multiple apparent Tafel slopes [28]. Considering in Eq. 2 the simplest case, namely intrinsic kinetic control described by Tafel polarization, and introducing the catalyst area enhancement factor a_s defined by Eq. 1, the superficial current density for methanol oxidation in the three-dimensional electrode becomes:

$$i = \gamma_c \frac{a_s}{\tau} \int_0^{\tau} i_{0,j} \exp\left(-\frac{2.3\eta_j}{b_j}\right) dx, \tag{3}$$

where b_j and $i_{0,j}$ are the local Tafel slope (V dec^{-1}) and exchange current density (A m^{-2}_{eff}) for methanol electrooxidation, respectively, at a point j in the electroactive zone. Thus, the spatial inhomogeneity of the electrode reaction rate in the three-dimensional electrode is accounted for.

Equation 3 shows that even if a_s is higher for PtRu/UGF compared to PtRu/RVC, there are a number of other variables that contribute also to the measured superficial current density i. An important factor is the catalyst penetration depth in the three-dimensional matrix determining the electroactive zone thickness τ and, moreover, the homogeneity of the PtRu catalyst composition across τ. Lycke and Gyenge studied this issue in the case of PtSn nanoparticle deposition on UGF using an electrochemical organosol method [18].

It was found that catalyst particles situated on the outer face of the substrate have different atomic ratios of the constitutive elements compared to particles situated inside, in the middle of the felt electrode. Hence, it is hypothesized that both τ and the local PtRu ratio could be different for PtRu/UGF versus PtRu/RVC in spite of an average 4:1 atomic ratio for both (Table 3). The catalyst composition gradient across the electroactive zone thickness will effect the kinetic parameters b_j and $i_{0,j}$ which in turn leads to different methanol oxidation rates (Eq. 3). Furthermore, differences in catalyst/support interaction between PtRu/UGF, PtRu/RVC and PtRu/Ti could also affect the kinetic parameters of methanol oxidation, such as electronic effects and/or different crystallographic features of the PtRu electrodeposit induced by the support. The crystallographic features, in terms of Eq. 3, will also impact the area based catalyst utilization efficiency γ_c since formation of crystalites richer in faces that are more active toward methanol oxidation will increase γ_c. These considerations point toward future experimental studies that are required in order to better understand the synergies between three-dimensional support and electrocatalytic activity.

3.4 Direct methanol fuel cell experiments

The extended reaction zone three-dimensional anodes with low PtRu catalyst load prepared using perforated counter electrodes and a deposition current density of 20 A m^{-2} (Table 3) were investigated in single-cell DMFCs operated at 333 K and fed on the anode side with 1 M CH_3OH and 0.5 M H_2SO_4 solution (Sect. 2.5). Figure 8 shows the cell voltage versus superficial current density, whilst Fig. 9 expresses the specific power output on area and catalyst mass basis, respectively.

The highest fuel cell peak power density at 333 K was obtained with the RVC substrate (486 W m^{-2} at 2,250 A m^{-2}), followed by UGF and lastly Ti mesh (Fig. 9a). While these results are in accordance with the voltammetry study (Sect. 3.3 and Fig. 7), the fuel cell results are also reflective of other phenomena, in addition to electrode kinetics. It is expected that the CH_3OH crossover to the cathode, compromising the cell voltage output due to the establishment of a mixed cathode potential, was the most severe in the case of the thin Ti mesh anode which also had the lowest PtRu load (only 2.8 g m^{-2}). On the other hand, the ohmic voltage drop loss was the lowest for Ti mesh support. The high methanol crossover for the PtRu/Ti system was reflected by the low open circuit cell voltage (i.e. 0.54 V (Fig. 8)) compared to PtRu/RVC and PtRu/UGF. Qi and Kaufman discussed the relationship between open circuit cell voltage and methanol crossover [29].

The power output on a catalyst mass basis was virtually identical for the three-anodes for currents up to about 200 A g^{-1} (Fig. 9b). At higher currents the performance of PtRu/RVC and PtRu/UGF leveled off, while the Ti mesh supported catalyst yielded a maximum catalyst mass specific power output of 50.4 W g^{-1} (Fig. 9b). Thus, the mass specific activities of the investigated anodes were comparable even though there was more than a four times difference in the PtRu load between Ti mesh (2.8 g m^{-2}) and RVC (12.0 g m^{-2}) in conjunction with obvious differences in substrate physico-chemical properties. In other words, increasing the anode catalyst load with the developed electrodeposition procedure on the various three-

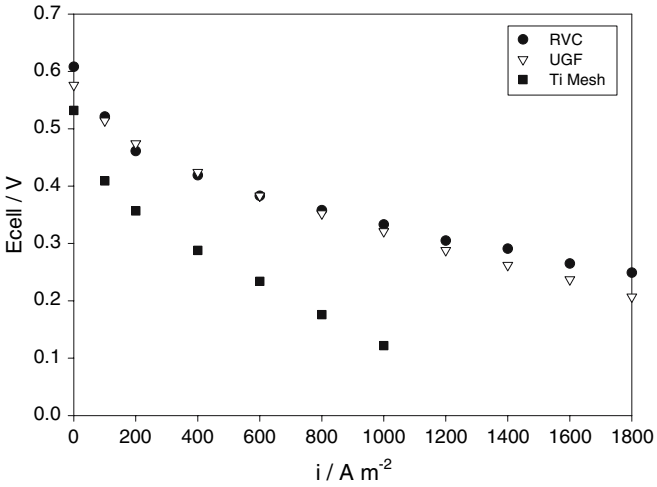

Fig. 8 Effect of three-dimensional anode with electrodeposited PtRu (see Table 3) on DMFC performance. Fuel: 1 M CH_3OH in 0.5 M H_2SO_4 at 2 mL min^{-1}. Cathode: 40 g Pt m^{-2}, dry O_2 fed at 2.5 bar and 500 mL min^{-1}. Temperature: 333 K

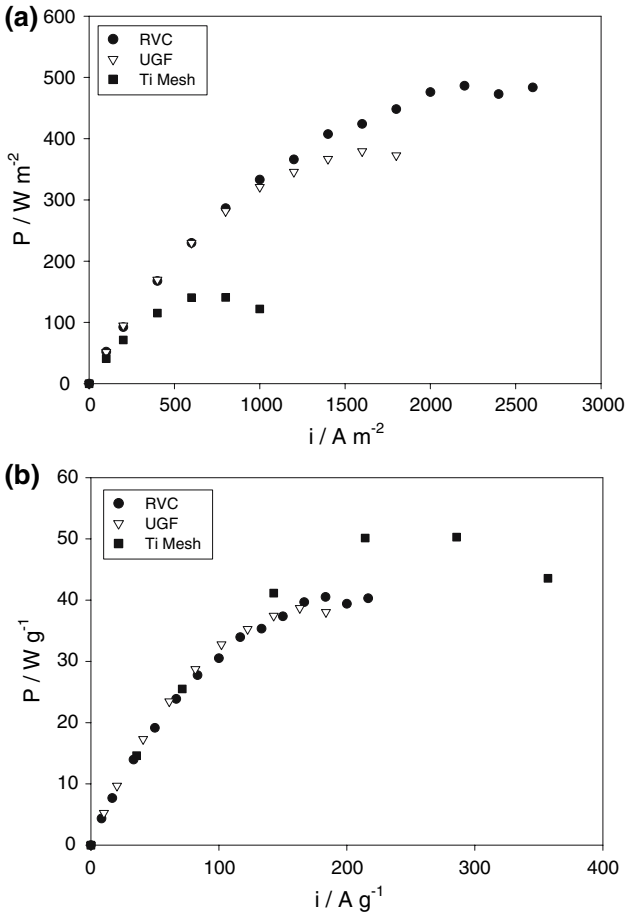

Fig. 9 DMFC power density. Three-dimensional anode support comparison. Conditions idem Fig. 8. (a) Area specific power density; (b) Mass specific power output

dimensional substrates did not lead to a decrease of catalyst mass specific activity.

Comparative fuel cell experiments were performed under identical operating conditions using a conventional gas diffusion anode with 10 and 40 g m^{-2} PtRu load supported on Vulcan XC-72. Table 4 summarizes the performance of the reference gas diffusion anodes obtained in-house together with representative literature results in order to better assess the effectiveness of the novel, extended reaction zone, three-dimensional anodes proposed in the present work. The literature results were selected such that to be comparable as much as possible with the conditions employed here, e.g. Nafion® 117 membrane, operating temperature of 333 K and PtRu catalysts with loads between 10 and 40 g m^{-2}. In all the selected reference DMFC experiments on the cathode side a gas diffusion electrode was employed with some variation regarding the cathode catalyst loading and O_2 pressure.

However, a major difference between our experimental conditions and pertinent literature relates to the use of 0.5 M H_2SO_4 for ionic conductivity. Most of the gas diffusion electrode studies in the literature were carried out without liquid ionic conductor (i.e. the proton exchange polymer supplies the ionic conductivity in the catalyst layer). The 0.5 M H_2SO_4 electrolyte while improves the ionic conductivity, which was essential especially for the RVC and UGF anode substrates, it could also enhance the CH_3OH crossover flux to the cathode due to increased electro-osmotic drag.

Table 4 shows that the performance of the conventional GDE used in the present work compares favorably with literature results, hence, validating the DMFC testing protocol. The catalyst mass specific peak power output of the reference GDE with a 1:1 Pt:Ru atomic ratio was 17.6 and 44.1 W g^{-1} at loads of 40 and 10 g m^{-2}, respectively. Thus, in the case of the GDE there was a significant loss in mass specific activity with catalyst load increase. The three-dimensional anodes gave maximum power outputs of 38.6–50.4 W g^{-1}. However, the PtRu atomic ratios obtained by the micellar media assisted deposition on the three-dimensional substrates were around 4:1, while a

Table 4 DMFC performance comparison between published data and results obtained in the present work

Anode catalyst layer	PtRu load (g m^{-2})	PtRu atomic ratio	Peak power output (W m^{-2})	Catalyst mass specific peak power output (W g^{-1})	Cathode pressure (bar_{abs})	Ref.
Anode type: conventional GDE						
PtRu/Vulcan XC-72	10.0	1.0:1	441	44.1	2.5	Present work
PtRu/Vulcan XC-72	40.0	1.0:1	703	17.6	2.5	Present work
PtRu/Vulcan XC-72	10.0	1.0:1	300	30.0	1.0	[30]
PtRu/Vulcan XC-72	35.0	1.0:1	510	14.6	1.0	[30]
PtRu/Vulcan XC-72	40.0	1.0:1	500	12.5	1.0	[31]
Unsupported PtRu	40.0	1.0:1	740	18.5	1.0	[32]
Anode type: three-dimensional substrate (extended reaction zone)						
RVC	12.0	3.6:1	486	40.5	2.5	Present work
UGF	9.8	4.0:1	379	38.6	2.5	Present work
Ti mesh	2.8	4.5:1	141	50.4	2.5	Present work
Ti mesh	40.0	2.3:1	450	11.3	1.0	[33]

Temperature: 333 K; Anode feed: 1 M CH_3OH—0.5 M H_2SO_4 (present work), 1 M CH_3OH in water (literature). Membrane: Nafion® 117

lower ratio (e.g. 1:1) is more favorable at 333 K [25–27, 33].

Therefore, the performance of the DMFC could be further improved with the extended anodic reaction zone provided by the three-dimensional substrate, if a 1:1 Pt:Ru atomic ratio can be achieved by the electrodeposition method. This was also proven experimentally by Bauer et al. in the case of a different type of graphite felt (i.e. compressed) subjected to an electrodeposition procedure carried out at high non-ionic surfactant concentration (i.e. 40 wt.%) [16].

There is scant literature information on the use of three-dimensional extended reaction zone anodes in direct fuel cells. Two recent studies employed Ti mesh substrates [21, 33]. Experiments by Allen et al. showed virtually no difference between the fuel cell polarization of PtRu/Ti mesh (10 g m^{-2}) and conventional GDE (10 g m^{-2} PtRu) in DMFC operated at 363 K [21]. The power output on both area and anode catalyst mass basis was nearly identical for the Ti mesh and GDE. Shao et al. on the other hand, working with 0.25 M, 0.5 M, and 1 M methanol concentration at 333 K as well as 363 K, observed that the Ti mesh supported PtRu performed better than the GDE in the high current density range, where mass transfer related effects gain significance [33]. The mass specific activities of their catalysts were lower than those obtained in the present study (Table 4).

Therefore, it can be concluded that the electrode preparation method using micellar media gives a PtRu catalyst morphology that provides high catalyst utilization on various three-dimensional substrates.

4 Conclusion

The electrodeposition of PtRu on three different three-dimensional substrates (Ti mesh, RVC and UGF) was studied using colloidal media. The resulting electrodes were tested for electrocatalytic activity toward methanol oxidation. The combination of Triton X-100/isopropanol aqueous micellar electrodeposition media and perforated counter electrodes yielded a mesoporous PtRu deposit morphology with high anode catalyst mass specific activity toward methanol oxidation as shown by both voltammetry and fuel cell experiments. The anode catalyst mass specific peak power output at 333 K was in the range 38.6–50.4 W g^{-1} corresponding to current loads of 170–220 A g^{-1}. The highest power densities were obtained with PtRu/RVC. It must be noted however, that RVC is a brittle material hence, the anode gasket thickness and cell compression have to be designed such that to avoid the crushing of the RVC. The electrode design proposed in the present work opens up the possibility of lowering the precious metal catalyst load in direct fuel cell anodes below 10 g m^{-2}. Future experiments will address the optimization of Pt:Ru atomic ratio and catalyst composition (e.g. using ternary formulations) for the specific conditions of three-dimensional electrode supports.

Acknowledgments The authors thank UBC BioImaging facility for the use of the SEM equipment and Dr. Anna Becalska of Vizon SciTec Inc. for ICP-AES. Financial support by the Natural Sciences and Engineering Research Council of Canada is gratefully acknowledged.

References

1. Arico AS, Srinivasan S Antonucci V (2001) Fuel Cells 1:133
2. Herrero E, Franaszczuk K, Wieckowski A (1994) J Phys Chem 98:5074
3. Iwasita T (2002) Electrochim Acta 47:3663
4. Anderson AB, Grantscharova E, Seong S (1996) J Electrochem Soc 143:2075
5. Wang H, Wingender C, Baltruschat H, Lopez M, Reetz MT (2001) J Electroanal Chem 509:163
6. Cao D, Lu G-Q, Wieckowski A, Wasileski SA, Nuerock M (2005) J Phys Chem B 109:11622
7. Gurau B, Smotkin E (2002) J Power Sources 112:339
8. Ling J, Savadogo O (2004) J Electrochem Soc 151:A1604
9. Park K-W, Choi J-H, Lee S-A, Pak C, Chang H, Sung Y-E (2004) J Catal 224:236
10. Gurau B, Viswanathan R, Liu R, Lafrenz TJ, Ley KL, Smotkin ES (1998) J Phys Chem B 102:9997
11. Ralph TR, Hards GA, Keating JE, Campbell SA, Wilkinson DP, Davis M, St-Pierre J, Johnson MC (1997) J Electrochem Soc 144:3845
12. Argyropoulos P, Scott K, Taama WA (1999) J Appl Electrochem 29:661
13. Mastragostino M, Missiroli A, Soavi F (2004) J Electrochem Soc 151:A1919
14. Hyeon T, Han S, Sung YE, Park KW, Kim YW (2003) Angew Chem Int Ed 42:4352
15. Wilkinson DP, Johnson MC, Colbow KM and Campbell SA (1999) US Patent 5,874,182, February 13
16. a) Bauer A, Gyenge EL and Oloman CW (2006) Electrochim Acta 51:5356; b) Bauer A, Gyenge EL and Oloman CW (2007) J Power Sources 167:281
17. Cheng TT, Gyenge EL (2006) Electrochim Acta 51:3904
18. Lycke DR, Gyenge EL (2007) Electrochim Acta 52:4287
19. McCusker LB, Liebau F, Engelhardt G (2001) Pure Appl Chem 73:381
20. Hodgson I, Oloman C (1999) Chem Eng Sci 54:5777
21. Allen RG, Lim C, Yang LX, Scott K, Roy S (2005) J Power Sources 143:142
22. Green CL, Kucernak A (2002) J Phys Chem B 106:1036
23. Teh HC, Ong GH, Ng SC, Gan LM (1980) Phys Lett A 78:487
24. Teh HC, Ong GH, Ng SC, Gan LM (1985) J Dispersion Sci Technol 6:255
25. Gasteiger HA, Markovic N, Ross PN, Cairns EJ (1994) J Electrochem Soc 141:1795
26. Gasteiger HA, Markovic N, Ross PN, Cairns EJ (1993) J Phys Chem 97:12020
27. Ross PN (1998) in Lipkowski J, Ross PN (eds) Electrocatalysis. Wiley-VCH, New York, p 66
28. Gyenge EL (2005) J Power Sources 152:105
29. Qi Z, Kaufman A (2002) J Power Sources 110:177
30. Baglio V, Blasi AD, Modica E, Creti P, Antonucci V, Arico AS (2006) Int J Electrochem Sci 1:71
31. Jiang R, Kunz HR, Fenton JM (2006) J Electrochem Soc 153:A1554
32. Gurau B, Smotkin ES (2002) J Power Sources 112:339
33. Shao ZG, Zhu F, Lin WF, Christensen PA, Zhang H (2006) Phys Chem Chem Phys 8:2720